

Multi-quantum-well nanowire heterostructures for wavelength-controlled lasers

FANG QIAN¹, YAT LI^{1*}, SILVIJA GRADEČAK^{1*}, HONG-GYU PARK^{1*}, YAJIE DONG¹, YONG DING², ZHONG LIN WANG^{2†} AND CHARLES M. LIEBER^{1,3†}

¹Department of Chemistry and Chemical Biology, Harvard University, Cambridge, Massachusetts 02138, USA

²School of Materials Science and Engineering, Georgia Institute of Technology, Atlanta, Georgia 30332, USA

³School of Engineering and Applied Sciences, Harvard University, Cambridge, Massachusetts 02138, USA

*Present address: Department of Chemistry and Biochemistry, University of California, Santa Cruz, California 95064, USA (Y.L.); Department of Materials Science and Engineering, Massachusetts Institute of Technology, Cambridge, Massachusetts 02139, USA (S.G.); Department of Physics, Korea University, Seoul 136-713, Korea (H.-G.P.)

†e-mail: zhong.wang@mse.gatech.edu; cml@cmliris.harvard.edu

Published online: 17 August 2008; doi:10.1038/nmat2253

Rational design and synthesis of nanowires with increasingly complex structures can yield enhanced and/or novel electronic and photonic functions^{1,2}. For example, Ge/Si core/shell nanowires have exhibited substantially higher performance as field-effect transistors³ and low-temperature quantum devices^{4,5} compared with homogeneous materials, and nano-roughened Si nanowires were recently shown to have an unusually high thermoelectric figure of merit⁶. Here, we report the first multi-quantum-well (MQW) core/shell nanowire heterostructures based on well-defined III-nitride materials that enable lasing over a broad range of wavelengths at room temperature. Transmission electron microscopy studies show that the triangular GaN nanowire cores enable epitaxial and dislocation-free growth of highly uniform (InGaN/GaN)_n quantum wells with $n = 3, 13$ and 26 and InGaN well thicknesses of 1–3 nm. Optical excitation of individual MQW nanowire structures yielded lasing with InGaN quantum-well composition-dependent emission from 365 to 494 nm, and threshold dependent on quantum well number, n . Our work demonstrates a new level of complexity in nanowire structures, which potentially can yield free-standing injection nanolasers.

Miniaturized multicolour lasers could be enabled with the development of a tunable-bandgap nanoscale gain medium that is coupled effectively into a small optical cavity. Free-standing nanowires have received considerable attention as nanolasers^{7–13}, where the semiconductor nanowires have functioned as both the gain medium and optical cavity. So far, nanowire lasers have been reported for several homogeneous binary semiconductors, including GaSb (refs 7,8), ZnO (ref. 9), GaN (refs 10,11), CdS (ref. 12) and ZnS (ref. 13), where the lasing wavelength in these studies corresponded to the fundamental bandgap energies of the respective homogeneous nanowire materials. The distinct nanowire bandgaps have led to lasing over a relatively wide range of discrete wavelengths but have not enabled continuous tuning in emission colour, although engineered lasing wavelength has been demonstrated in alloy nanoribbon systems^{14,15}. More generally, we

believe that a decoupling of studies of the gain medium and cavity could offer advantages over homogeneous nanowire structures for designed laser wavelength output in parallel with independent optimization of the cavity.

To address this general concept in nanolasers, we have focused on group-III nitride multi-quantum-well (MQW) nanowire heterostructures. Our MQW nanowire structure design (Fig. 1a) consists of a GaN nanowire core, which functions as the primary part of the optical cavity^{10,11}, and epitaxial InGaN/GaN MQW shells, which serve as the composition-tunable gain medium. An MQW structural motif was chosen because of its potential as a low-threshold and tunable gain medium^{16,17}, although such complex shell structures have not been previously reported for nanowire materials. In comparison with planar MQW structures, nanowire heterostructure growth has the potential advantage of a dislocation-free and unstrained GaN nanowire ‘substrate’ but has the added complexity of distinct lateral facets that could affect, for example, growth rates.

MQW nanowire heterostructures with 3–26 quantum wells were prepared by metal–organic chemical vapour deposition, where the GaN nanowire core was elaborated in a metal-nanocluster-catalysed growth step followed immediately by MQW shell deposition without removal from the growth reactor (see the Methods section). Transmission electron microscopy (TEM) data recorded with the electron beam perpendicular to the axis of a typical MQW nanowire (Fig. 1b) reveals that the structure is single crystalline and dislocation free; measurements made on 50 independent samples showed similar results. High-resolution TEM images and electron diffraction data (Fig. 1c) further confirm the single-crystalline structure, demonstrate that the nanowires grow along the $\langle 11\bar{2}0 \rangle$ direction and show that nanowire surfaces are atomically smooth. The smooth interfaces are consistent with the growth of continuous quantum-well shells on the GaN nanowire core, and are also expected to reduce optical losses at the nanowire–air interface, which is an important factor for reducing threshold in nanowire lasers¹¹.

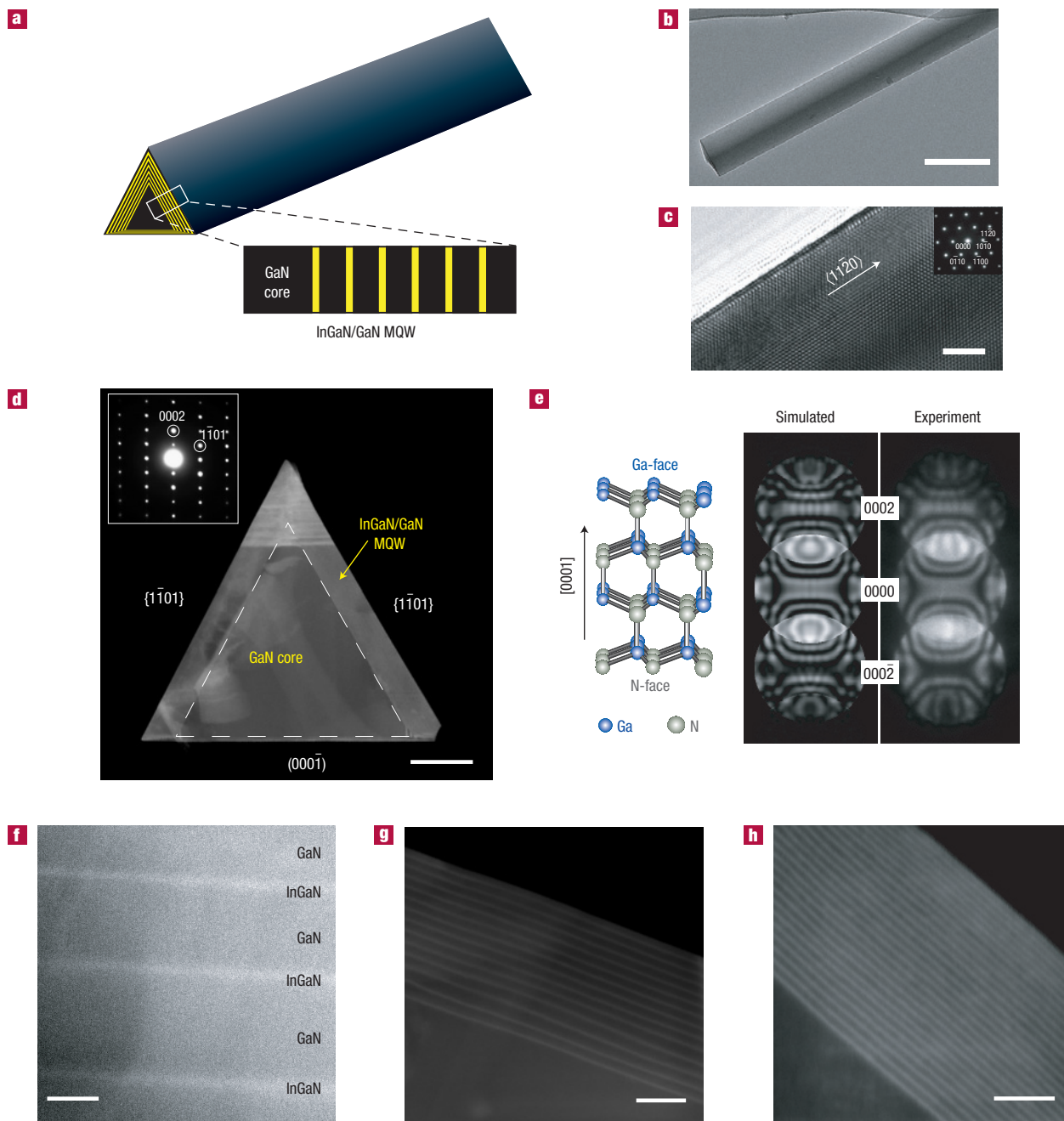


Figure 1 InGaN MQW nanowire structures. **a**, Schematic diagram of an MQW nanowire and magnified cross-sectional view of a nanowire facet highlighting InGaN/GaN MQW structure. The InGaN layer is indicated in yellow colour. **b**, Low-resolution TEM image of an MQW nanowire structure. The scale bar is 500 nm. **c**, High-resolution TEM image of an MQW nanowire structure taken along the [0001] zone axis. The white arrow indicates the $\{11\bar{2}0\}$ direction (along the nanowire axis). The scale bar is 5 nm. Inset: Corresponding electron diffraction pattern indexed for the [0001] zone axis. **d**, Dark-field cross-sectional STEM image recorded along the $[11\bar{2}0]$ zone axis of a 26MQW nanowire structure. Dashed lines indicate core/shell interface. The scale bar is 100 nm. Inset: Corresponding electron diffraction pattern indexed for the $[11\bar{2}0]$ zone axis. **e**, Left: Schematic GaN wurtzite crystal structure viewed along the $[11\bar{2}0]$ direction. Right: Simulated and experimental CBED patterns along the $[11\bar{0}0]$ zone axis from a 216-nm-thick MQW nanowire cross-sectional sample. **f–h**, Dark-field cross-sectional STEM images recorded along the $[11\bar{2}0]$ direction at the $\{11\bar{0}1\}$ facet of 3MQW (**f**), 13MQW (**g**) and 26MQW (**h**) nanowire structures; scale bars are 20, 50, and 20 nm, respectively.

We have exploited cross-sectional TEM imaging of the MQW nanowire structures to visualize directly the quantum-well stacking on the nanowire lateral facets. Representative dark-field scanning TEM (STEM), electron diffraction and energy-dispersive X-ray spectroscopy (EDS) data recorded from a 26-period InGaN/GaN

quantum-well (26MQW) sample (Fig. 1d) highlight several key points. First, analysis of these results shows that epitaxial growth occurs on the two distinct facet types of the triangular core; that is, the two crystallographically equivalent $\{11\bar{0}1\}$ planes and a $\{0001\}$ plane, which were determined by the electron

diffraction pattern indexed along the $[1\bar{1}20]$ axis (Fig. 1d, inset). Second, these data show that the overall InGaN/GaN shell structure on the two $\{1\bar{1}01\}$ facets is thicker, ~ 65 nm, than on the $\{0001\}$ facet, ~ 10 nm. High-magnification data (Fig. 1h and Supplementary Information, Fig. S1) show clearly the 26-period InGaN quantum-well structure on the $\{1\bar{1}01\}$ facets, whereas no quantum-well contrast variation was observed on the $\{0001\}$ facet. Third, EDS measurements (Supplementary Information, Fig. S2) further confirm this difference in shell thickness with a well-defined In signal recorded from the MQW shell on the $\{1\bar{1}01\}$ facets but no detectable In signal from the thinner shell on the $\{0001\}$ facet. We address further this difference below. Last, we note that contrast variation can also be observed at the intersection between the $\{1\bar{1}01\}$ facets in some MQW nanowire samples. Preliminary high-resolution TEM analysis of a 26MQW sample (Supplementary Information, Fig. S3) suggests that these features arise from stacking faults at this intersection, although further studies will be required to understand fully this interesting structural feature.

To understand further the MQW growth differences on the two $\{1\bar{1}01\}$ lateral facets versus the $\{0001\}$ facet of the nanowire, we carried out convergent-beam electron diffraction (CBED). Comparison of experimental and simulated¹⁸ (see the Methods section) CBED patterns (Fig. 1e) suggests that the $\{0001\}$ bottom facet of the MQW nanowire is an N-polarity face. Interestingly, previous studies of planar growth have reported that an N-face has a much slower growth rate than a Ga-face¹⁹, and could thus explain the difference in shell growth for our nanowires. Given the more rapid and controlled growth on the $\{1\bar{1}01\}$ nanowire facets, we have focused on growth of multiple-quantum-well structures on these facets to explore limits of synthetic control and to prepare nanolaser structures in which the gain medium is tuned. Notably, by varying the growth time and temperature and total repeat periods during the MQW deposition (see the Methods section), we were able to vary the InGaN/GaN quantum-well unit thicknesses, the In composition and total quantum-well numbers. Cross-sectional STEM images of three distinct MQW nanowires used in our subsequent studies (Fig. 1f–h) show structures with resolvable 3, 13, and 26 periods, quantum-well thicknesses of about 2.4, 3.0 and 1.5 nm and average GaN barrier thicknesses of about 40, 10 and 1 nm, respectively. The In composition control was confirmed by optical studies to be discussed later.

We have further investigated the detailed structure of the InGaN/GaN quantum-well repeat by acquiring high-resolution bright-field images from an independent 26MQW nanowire cross-section sample. A lattice-resolved image of the 26MQW structure on the $\{1\bar{1}01\}$ nanowire facet (Fig. 2a) reveals homogeneous quantum-well deposition as discussed above. High-magnification data of several quantum wells (Fig. 2b) reveal that the InGaN/GaN interfaces are atomically sharp, with the InGaN quantum-well thickness estimated to be ≤ 1 nm and approaching the growth limit of several monolayers. In addition, two-dimensional Fourier transforms from the MQW region (Fig. 2b, inset) exhibit no splitting of reciprocal lattice peaks, suggesting that there is no strain relaxation at the InGaN/GaN heterointerfaces. These TEM results confirm that we can prepare dislocation-free MQW nanowire heterostructures with InGaN quantum-well thicknesses similar to or smaller than the Bohr radius, ~ 3 nm, for InGaN (ref. 20).

We have characterized the optical properties of the new core/MQW-shell nanowire heterostructures using photoluminescence and modelling studies. Photoluminescence images and spectra from individual 26MQW nanowires containing different In compositions (Fig. 3a,b) reveal several points. First, the InGaN emission peak redshifts from 382 to 440 to 484 nm (Fig. 3b) with increasing In composition. The InGaN quantum-well compositions estimated²¹ from the emission data, $\text{In}_{0.05}\text{Ga}_{0.95}\text{N}$,

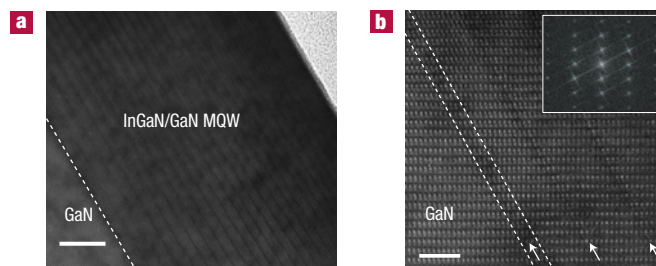


Figure 2 High-resolution TEM of nanowire MQWs. **a**, Bright-field TEM image of a typical 26MQW nanowire cross-section. The dashed line indicates the heterointerface between the core and shell. The scale bar is 10 nm. **b**, Enlarged TEM image of MQWs in **a**. White arrows highlight InGaN quantum-well positions. The dashed line outlines the interface between an InGaN quantum well and adjacent GaN quantum barriers. The scale bar is 2 nm. Inset: Two-dimensional Fourier transforms of the entire image.

$\text{In}_{0.16}\text{Ga}_{0.84}\text{N}$ and $\text{In}_{0.23}\text{Ga}_{0.77}\text{N}$, are consistent with that expected based on our previous studies of InGaN shell growth²². The peak broadening with In% is consistent with InGaN planar structures²³. Second, the photoluminescence images show strong emission from the nanowire bodies where excitation occurs, and also from the nanowire ends, which indicates good waveguiding in the core/MQW-shell structure. Third, the images also show that most In-rich nanowires exhibited spontaneous bending. We attribute this behaviour to the non-symmetrical shell coating, where larger strains are generated on $\{1\bar{1}01\}$ versus $\{000\bar{1}\}$ facets. It may be interesting in the future to quantify the relationship between In composition and bending in these structures, and thus the possible strain relaxation through mechanical bending. Last, we note that no impurity or defect-related emission was observed at longer wavelengths in the photoluminescence spectra, consistent with the high degree of structural order determined from our high-resolution TEM analyses.

Excitation power-dependent studies of a representative 26MQW nanowire structure were also carried out, as shown in Fig. 3c. At low power density (245 kW cm^{-2}), we observed a relatively broad spontaneous emission peak centred at 448 nm. As power density increased, the end emission intensity increased rapidly and became dominant. Above a threshold of 900 kW cm^{-2} , this spontaneous emission peak collapsed into several well-defined narrow peaks centred around 438 nm. The full-width at half-maximum of these peaks was less than 0.8 nm, limited by the spectral resolution of our detection system and indicative of longitudinal modes in the nanowire cavity. To confirm this assumption, we calculated the mode spacing using $\Delta\lambda = \lambda^2 / (2n_e L)$ (ref. 24), where λ is the emission wavelength, n_e is the effective refractive index and L is the nanowire cavity length. For $\lambda = 438$ nm, $n_e = 2.625$ (ref. 25) and $L = 50 \mu\text{m}$, the predicted mode spacing is around 0.73 nm, which is consistent with the measured mode spacing 0.72–0.82 nm. These features together with the observed characteristic nonlinear spectrally integrated output power versus pump power density (Fig. 3c, inset) are clear indications of lasing behaviour²⁶. Comparison of the measured output power data with a fit derived from the rate equations (see the Supplementary Information) yields a spontaneous emission factor, β , of 0.03. This value is consistent with that reported for InGaN MQW lasers²⁷. The blueshift of lasing peaks relative to the spontaneous emission is a distinct feature of InGaN MQW lasers, which has been attributed to band filling and/or photo-induced screening of internal electric fields^{22,28,29}.

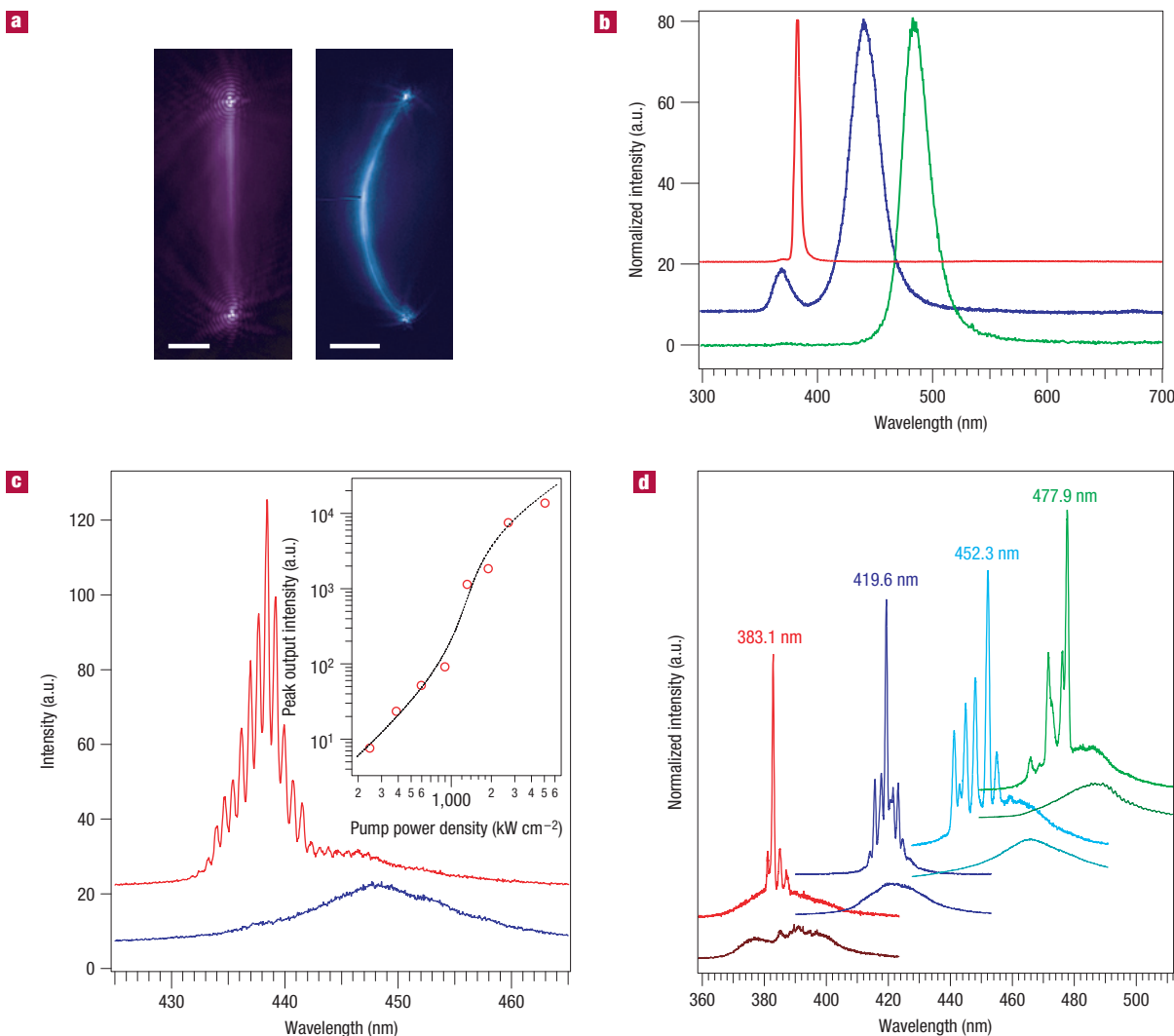


Figure 3 MQW nanowire photoluminescence. **a**, Photoluminescence images (false colour) recorded from GaN/In_{0.05}Ga_{0.95}N (left) and GaN/In_{0.23}Ga_{0.77}N (right) MQW nanowire structures. Scale bars are 5 μm . **b**, Normalized spectra collected from three representative 26MQW nanowire structures with increasing In composition; excitation power density $\sim 150 \text{ kW cm}^{-2}$. **c**, Photoluminescence spectra of a 26MQW nanowire recorded at excitation power densities of 250 and 1,300 kW cm^{-2} , respectively. Spectra are offset for clarity. Inset: Log–log plot of output power versus pump power density. Red open circles are experimental data points and the dashed line is the fit calculated with the rate equations. **d**, Normalized photoluminescence spectra collected from four representative 26MQW nanowire structures with increasing In composition pumped at $\sim 250 \text{ kW cm}^{-2}$ and $\sim 700 \text{ kW cm}^{-2}$, respectively. Spectra are offset for clarity.

In addition, we have investigated power-dependent excitation and resulting photoluminescence from MQW nanowire structures as a function of In% in the InGaN quantum well. Significantly, normalized photoluminescence spectra acquired from four representative MQW nanowire structures with increasing In%, below and above thresholds (Fig. 3d), show lasing behaviour with peak maxima at 383, 420, 452 and 478 nm, spanning a substantial portion of the ultraviolet to visible region of the electromagnetic spectrum. The threshold power densities for these four MQW nanowire lasers are all below 700 kW cm^{-2} . Finally, preliminary studies of a higher In composition 26MQW nanowire structure (Supplementary Information, Fig. S4) yielded power-dependent photoluminescence spectra suggestive of lasing at 494 nm. Although further studies will be needed to characterize fully this MQW nanowire composition regime, this is to the best of our knowledge the longest wavelength lasing for an

InGaN-based material³⁰. Overall, these data demonstrated that our concept and realization of MQW nanowire heterostructures yield unprecedented tunability for nanowire-based lasers at room temperature.

Given the unique geometry of our MQW nanowire lasers (Fig. 4a), where the MQW gain medium is separated from the nanowire core in contrast to previous homogeneous nanowire systems^{7–13}, we have investigated how the number of quantum wells in the gain medium affects the laser threshold. For conventional rate equation analysis, the threshold can be approximated as¹⁷:

$$L_{\text{th}}^{(N_w)} \sim \frac{qN_w V_1 B N_{\text{tr}}^2}{\eta_i} e^{2\omega/Qv_g N_w \Gamma_1 g_0},$$

where L_{th} is the threshold, N_w is the number of quantum wells, V_1 is the active volume per well, B is the bimolecular recombination coefficient, g_0 is the differential gain, N_{tr} is the transparent carrier

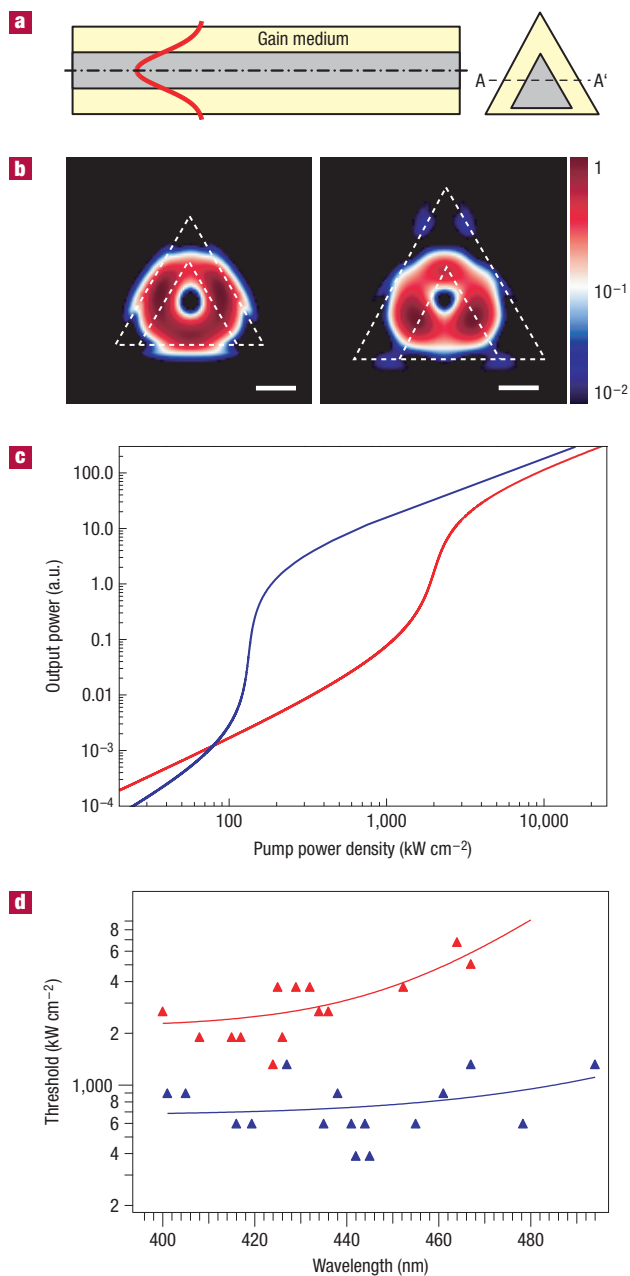


Figure 4 MQW nanowire lasing threshold. **a**, Schematic diagram of an optical mode along the nanowire axis. Cross-sectional top view of a MQW nanowire taken along the A-A' position indicated in the end-on view at the right. The MQW shell and GaN core are indicated in yellow and grey, respectively. The red curve represents the optical mode and the dashed-dotted line indicates the middle of the nanowire longitudinal cavity. **b**, FDTD simulation of the dominant laser mode in 13MQW and 26MQW nanowire structures. White lines indicate the nanowire profile and the core/shell interface. The scale bar is 100 nm. **c**, Calculated light-in versus light-out curve for 13MQW (red) and 26MQW (blue) nanowire structures. **d**, Measured lasing thresholds as a function of wavelength for 13MQW (red) and 26MQW (blue) nanowires. Solid symbols correspond to experimental data and lines are guides for the eyes.

density, Γ_1 is the optical confinement factor per well, Q is the quality factor, ω is the frequency of the resonant mode, v_g is the group velocity and η_i is the absorption ratio in quantum wells.

In this way, we have compared relative threshold ratios for 13 and 26MQW nanowire structures by determining the quality factor, Q , and confinement factor, Γ , using three-dimensional finite-difference time-domain (3D-FDTD) calculations because other parameters remain approximately constant. The modes with the highest Q (Fig. 4b) exhibited a characteristic central intensity node and substantial overlap with MQW gain medium. The specific values of Q and Γ for these modes obtained from the calculations for the 26MQW nanowire structure, ($Q = 2,485$ and $\Gamma = 0.240$), were larger than those values for the 13MQW nanowire, ($Q = 656$ and $\Gamma = 0.122$), thus indicating that the threshold for lasing should be lower in the 26MQW structures. This conclusion was further analysed by calculating the light input–output curves (see Supplementary Information, Methods) as shown in Fig. 4c. These data show that L_{th} is about 14 times lower for the 26MQW versus 13MQW nanowire structures at a lasing wavelength of 450 nm.

Finally, the experimentally determined lasing threshold for a series of 13MQW and 26MQW nanowire structures (Fig. 4d) shows that L_{th} is 4–10 times lower for the 26 versus 13 MQW structures across the 400–500 nm wavelength region, in good agreement with our numerical calculations. Variation in L_{th} within the same MQW structure type reflects expected differences of individual nanowire cavities. The thresholds for the InGaN MQW nanowire lasers are comparable to the planar InGaN MQW lasers pumped at similar excitation energies²⁹, although they are higher than the best reported value¹¹ for homogeneous GaN nanowires. We attribute this last difference primarily to smaller confinement factors in the present MQW structures but believe that future nanowire structure optimization can reduce threshold values (see the Supplementary Information). Significantly, we note that the 26MQW nanowire lasing threshold exhibits little wavelength dependence, in contrast to typical InGaN MQW planar structures, where lasing thresholds exhibit an exponential increase with emission wavelength³¹. This has been attributed to the deterioration of material quality with increasing In composition³¹, which we believe is alleviated in our case as the MQW nanowire structures are dislocation-free single crystals.

In summary, we have reported controlled synthesis of the first MQW core/shell nanowire heterostructures based on well-defined III-nitride materials. TEM studies have demonstrated that the triangular single-crystalline GaN nanowire cores enable epitaxial and dislocation-free growth of highly uniform $(\text{InGaN}/\text{GaN})_n$ quantum wells with $n = 3, 13$ and 26 and InGaN well thicknesses of 1–3 nm. Optical studies of individual MQW nanowire structures further demonstrated lasing with InGaN quantum-well composition-dependent emission from 365 to 494 nm. Calculations exploring this new nanowire laser architecture have shown that laser threshold is reduced for increasing n -value owing to higher Q and Γ , and this prediction was confirmed by experimental studies showing a 4–10-fold threshold reduction in 26 versus 13 MQW structures. There are also areas that could benefit from further effort, including coupled synthesis and structural analyses designed to push the limit of In composition in the quantum wells and to define differences in growth for the unique nanowire versus planar geometry. Finally, we believe it will be interesting to implement an extra level of complexity with p-type AlGaIn/GaN shells, as this could enable the realization of free-standing nanowire injection nanolasers.

METHODS

NANOWIRE SYNTHESIS

MQW nanowire structures were synthesized on an *r*-plane sapphire substrate in a metal–organic chemical vapour deposition reactor (Thomas Swan Scientific Equipment Ltd) using trimethylgallium (TMG), trimethylindium

and ammonia (NH₃) as Ga, In and N sources, respectively, and nickel nanoclusters as core growth catalysts. GaN cores were grown in hydrogen at 950 °C and 700 torr for 4,800 s using TMG (22 μmol min⁻¹) and NH₃ (67 mmol min⁻¹). Under this condition, most GaN cores were of 100–200 nm size and 20–40 μm length. Subsequently, the growth conditions were altered to favour homogeneous MQW shell deposition onto the nanowire surface versus axial addition at the catalyst site. MQW shell growth was carried out in constant NH₃ flow (290 mmol min⁻¹) in nitrogen at 400 torr. An InGaN quantum well was deposited at 600–800 °C for 20–30 s using TMG (5.3 μmol min⁻¹) and trimethylindium (6.5 μmol min⁻¹). The temperature was varied to achieve the desired In% as higher deposition temperature leads to less efficient In incorporation. A GaN quantum barrier was grown at 830 °C for 10–360 s using TMG (12.3 μmol min⁻¹). A purge time of 60 s was applied between layer depositions. This quantum well/quantum barrier growth unit was alternated for 3, 13, 26 cycles, respectively, to achieve 3, 13 and 26 MQW nanowire structures.

ELECTRON MICROSCOPY

For conventional TEM studies, nanowires were first sonicated from growth substrate and then dispersed onto Cu/lacey-carbon TEM grids. For cross-section TEM studies, nanowires were aligned on Thermanox plastic slips by direct transfer from the growth substrate³², and embedded into an Eponate–Araldite epoxy resin. Embedded samples were cut perpendicular to the nanowire axis into 50–200-nm-thick slices using a diamond ultramicrotome knife and then transferred onto TEM grids. STEM images were obtained using a field-emission TEM/STEM (JEOL 2010F) operated at 200 kV. High-resolution bright-field TEM imaging was carried out using a JEOL 4000EX TEM operated at 400 kV. EDS elemental mapping was conducted using a VG HB603 STEM.

The experimental CBED patterns were taken along the (1100) zone axis of a 216-nm-thick cross-sectional nanowire sample 30° from the nanowire growth direction using a JEOL2100 TEM operating at 200 kV. By underfocusing and overfocusing the condenser lens, we verified that no 180° rotation is present between the bright-field image and the corresponding diffraction pattern. The numerical CBED simulations were carried out using the JEMS software for the GaN (1100) zone axis with 50 zero-order reflections and zero defocus. A series of CBED patterns was calculated with thicknesses ranging from 200 to 280 nm with 2 nm steps and the pattern best matching the experimental data was selected. Zone-axis CBED patterns present significant differences in (0001) and (0001̄) diffraction discs that enable unambiguous diffraction labelling and polarity determination.

OPTICAL MEASUREMENTS

Room-temperature optical studies of individual MQW nanowire structures were carried out using home-built far-field epifluorescence apparatus using a Q-switched Nd:YVO₄ laser (266 nm, 35 kHz repetition rate and 7 ns pulse duration) as the excitation source. The excitation laser was focused by a microscope objective (numerical aperture 0.65) to a 30 μm spot onto nanowires dispersed onto an oxidized Si (600 nm thermal SiO₂) substrate. Photoluminescence data were recorded using a 300 mm spectrometer (150 lines mm⁻¹ grating) and a liquid-nitrogen-cooled CCD (charge-coupled device) detector; images were obtained with the same system by replacing the grating with a mirror.

FDTD CALCULATION

The full-vector time-dependent Maxwell's equations were solved using the 3D-FDTD method on a computational grid with absorbing (perfectly matched layers) boundary conditions. The computation grid size is 12.5 nm. A core/shell nanowire with triangular cross-section was introduced in the calculation domain with size of 1.5 μm × 1.5 μm × 12 μm. The same structural parameters of the nanowire as those obtained from TEM analysis in the manuscript were used in our simulation. Only the shorter nanowire length of 10 μm was assumed to save computation time. Average refractive indices of the core and the shell of the nanowire were 2.537 and 2.625, respectively. To excite resonant modes in the nanowire cavity, temporally Gaussian dipole sources with the lasing wavelength are introduced at several arbitrary positions of the nanowire and then the simulation stores the time evolution of the electromagnetic fields. The simulation results are Fourier transformed to determine the resonant frequency. Q and Γ of each excited mode are computed from the temporal attenuation of

electromagnetic energy and the ratio of electric field intensity overlapped with the active region, respectively.

Received 4 March 2008; accepted 15 July 2008; published 17 August 2008.

References

- Lieber, C. M. & Wang, Z. L. Functional nanowires. *Mater. Res. Soc. Bull.* **32**, 99–104 (2007).
- Li, Y., Qian, F., Xiang, J. & Lieber, C. M. Nanowire electronic and optoelectronic devices. *Mater. Today* **9**, 18–27 (2006).
- Xiang, J. *et al.* Ge/Si nanowire heterostructures as high-performance field-effect transistors. *Nature* **441**, 489–493 (2006).
- Xiang, J., Vidan, A., Tinkham, M., Westervelt, R. M. & Lieber, C. M. Ge/Si nanowire mesoscopic Josephson junctions. *Nature Nanotechnol.* **1**, 208–213 (2006).
- Hu, Y. *et al.* A Ge/Si heterostructure nanowire-based double quantum dot with integrated charge sensor. *Nature Nanotechnol.* **2**, 622–625 (2007).
- Hochbaum, A. I. *et al.* Rough silicon nanowires as high performance thermoelectric materials. *Nature* **451**, 163–168 (2008).
- Mao, S. S. Nanolasers: lasing from nanoscale quantum wires. *Int. J. Nanotechnol.* **1**, 42–85 (2004).
- Chin, A. H. *et al.* Near-infrared semiconductor subwavelength-wire lasers. *Appl. Phys. Lett.* **88**, 163115 (2006).
- Huang, M. H. *et al.* Room-temperature ultraviolet nanowire nanolasers. *Science* **292**, 1897–1899 (2001).
- Johnson, J. *et al.* Single gallium nitride nanowire lasers. *Nature Mater.* **1**, 106–110 (2002).
- Gradecak, S., Qian, F., Li, Y., Park, H.-G. & Lieber, C. M. GaN nanowire lasers with low lasing thresholds. *Appl. Phys. Lett.* **87**, 173111 (2005).
- Duan, X., Huang, Y., Agarwal, R. & Lieber, C. M. Single-nanowire electrically driven lasers. *Nature* **421**, 241–245 (2003).
- Zapfen, J. *et al.* Room-temperature single nanoribbon lasers. *Appl. Phys. Lett.* **84**, 1189–1191 (2004).
- Liu, Y. K. *et al.* Wavelength-controlled lasing in Zn,Cd_{1-x}S single-crystal nanoribbons. *Adv. Mater.* **17**, 1372–1377 (2005).
- Liu, Y. K., Zapfen, J. A., Shan, Y. Y., Tang, H. & Lee, S. T. Wavelength-tunable lasing in single-crystal Cd_{1-x}Se_x nanoribbons. *Nanotechnology* **18**, 365606 (2007).
- Asada, M., Miyamoto, Y. & Suematsu, Y. Gain and the threshold of three dimensional quantum-box lasers. *IEEE J. Quantum Electron.* **22**, 1915–1921 (1986).
- Coldren, L. A. & Corzine, S. W. *Diode Lasers and Photonic Integrated Circuits* (Wiley, New York, 1995).
- <<http://cimewww.epfl.ch/people/stadelmann/jemsWebSite/jems.html>>.
- Northrup, J. E. & Neugebauer, J. Strong affinity of hydrogen for the GaN (0001̄) surface: Implications for molecular beam epitaxy and metalorganic chemical vapour deposition. *Appl. Phys. Lett.* **85**, 3429–3431 (2004).
- Ramvall, P., Riblet, P., Nomura, S., Aoyagi, Y. & Tanaka, S. Efficient observation of narrow isolated photoluminescence spectra from spatially localized excitons in InGa_{1-x}N quantum wells. *Jpn. J. Appl. Phys.* **44**, L1381–L1384 (2005).
- Wu, J. & Walukiewicz, W. Band gaps of InN and group III nitride alloys. *Superlatt. Microstruct.* **34**, 63–75 (2003).
- Qian, F., Gradecak, S., Li, Y., Wen, C.-Y. & Lieber, C. M. Core/multishell nanowire heterostructures as multicolor, high-efficiency light-emitting diodes. *Nano Lett.* **5**, 2287–2291 (2005).
- Nakamura, S., Pearton, S. & Fasol, G. *The Blue Laser Diode: The Complete Story* (Springer, Berlin, 2000).
- Silfvast, W. T. *Laser Fundamentals* (Cambridge Univ. Press, Cambridge, 2005).
- Martin, J. A. & Sanchez, M. Comparison between a graded and step-index optical cavity in InGa_{1-x}N MQW laser diodes. *Semicond. Sci. Technol.* **20**, 290–295 (2005).
- Chuang, S. L. *Physics of Optoelectronic Devices* (Wiley, New York, 1995).
- Tawara, T., Gotch, H., Akasaka, T., Kobayashi, N. & Saitoh, T. Low-threshold lasing of InGa_{1-x}N vertical-cavity surface-emitting lasers with dielectric distributed Bragg reflectors. *Appl. Phys. Lett.* **83**, 830–832 (2003).
- Kawakami, Y. *et al.* Inhomogeneity and emission characteristics of InGa_{1-x}N. *J. Phys. Condens. Matter* **13**, 6993–7010 (2001).
- Yablonskii, G. P. *et al.* Luminescence and lasing in InGa_{1-x}N/GaN multiple quantum well heterostructures grown at different temperatures. *Appl. Phys. Lett.* **85**, 5158–5160 (2004).
- Takahashi, K., Yoshikawa, A. & Sandhu, A. *Wide Bandgap Semiconductors: Fundamental Properties and Modern Photonic and Electronic Devices* (Springer, New York, 2007).
- Yablonskii, G. P. *et al.* Multiple quantum well InGa_{1-x}N/GaN blue optically pumped lasers operating in the spectral range of 450–470 nm. *Phys. Status Solidi A* **188**, 79–82 (2001).
- Javey, A., Nam, S., Friedman, R. S., Yan, H. & Lieber, C. M. Layer-by-layer assembly of nanowires for three-dimensional, multifunctional electronics. *Nano Lett.* **7**, 773–777 (2007).

Supplementary Information accompanies this paper on www.nature.com/naturematerials.

Acknowledgements

The authors thank C. J. Barrelet and Y. N. Wu for helpful discussions, P. Stadelmann for providing JEMS simulation software, R. Schalek for help with ultramicrotomy and A. J. Garratt-Reed for assistance in EDS elemental mapping measurements. This work was supported by the Air Force Office of Scientific Research (C.M.L.) and the Department of Energy Basic Energy Sciences, DE-FG02-07ER46394, (Z.L.W.).

Author contributions

F.Q., Y.L. and Y.J.D. synthesized the nanowire structures. Y.L. and Y.D. carried out TEM characterization, S.G. carried out CBED studies and analysis, F.Q. carried out optical measurements and H.-G.P. carried out modelling studies. All authors contributed to the design of the experiments and data analysis. F.Q. and C.M.L. wrote the paper and all authors contributed to manuscript revisions.

Author information

Reprints and permission information is available online at <http://npg.nature.com/reprintsandpermissions>. Correspondence and requests for materials should be addressed to Z.L.W. or C.M.L.